Dissipation of isotropic turbulence and length-scale measurements through the wave roller in laboratory spilling waves

K. Govender
Department of Physics, University of KwaZulu-Natal, Durban, South Africa

G. P. Mocke
Marine Works Unit, Dubai Municipality, Dubai, United Arab Emirates

M. J. Alport
School of Pure and Applied Physics, University of KwaZulu-Natal, Durban, South Africa

Received 3 December 2003; revised 27 May 2004; accepted 22 June 2004; published 27 August 2004.

[1] The measurement of turbulence dissipation rates and length scales associated with three-dimensional isotropic structures under spilling waves breaking in a laboratory surf zone is presented. Dissipation rates were estimated from the spectral characteristics of the turbulence velocities in the inertial subrange, and length scales were estimated using measurements of the turbulent kinetic energy and dissipation rate. The spatial velocity flow fields for the above analysis were measured using digital correlation image velocimetry. A unique set of measurements that spans the entire water column, including the aerated portion near the crest of the wave, is presented. Dissipation rates were found to reach a maximum above the effective trough level, with over 80% of the depth integrated dissipation occurring in this upper zone. The total depth integrated turbulence dissipation rate is found to be up to an order of magnitude smaller than the local rate of wave energy dissipation due to breaking, the primary turbulence production source. The length scale is found to increase in magnitude below the surface, consistent with the idea that turbulence production occurs above the trough level in the vicinity of the wave roller and is transported downward toward the bed. *INDEX TERMS:* 4546 Oceanography: Physical: Nearshore processes; 4568 Oceanography: Physical: Turbulence, diffusion, and mixing processes; 4558 Oceanography: Physical: Sediment transport; *KEYWORDS:* digital correlation image velocimetry, dissipation rates, length scales, turbulent kinetic energy, wave breaking, surf zone

Citation: Govender, K., G. P. Mocke, and M. J. Alport (2004), Dissipation of isotropic turbulence and length-scale measurements through the wave roller in laboratory spilling waves, *J. Geophys. Res.*, *109*, C08018, doi:10.1029/2003JC002233.

1. Background

[2] The nearshore surf zone is characterized by wave breaking as deep water waves move into shallow waters. The wave energy is converted into mean currents and turbulent kinetic energy. The turbulent motion of the fluid is responsible for the transfer of momentum to the bottom sediment, resulting in sediment suspension. The suspended sediments are then transported and deposited elsewhere by the mean currents. This action results in the erosion and deposition of sediments along the coastline. A quantitative knowledge of the turbulence levels present in the surf zone is therefore essential for the theoretical prediction of the sediment transport dynamic and associated changes.

[3] The theoretical analysis of turbulence can be performed via the Reynolds decomposition of the variables in the Navier-Stokes equation into their mean and fluctuating parts. Time averaging then gives the equations for the mean flow, kinetic energy of the mean, and turbulent parts of the flow, etc.

[4] The behavior of the turbulent kinetic energy (TKE), k, which is defined as $k = (1/2)\ \langle u_i' u_i' \rangle$, is described by the following equation:

$$\frac{\partial k}{\partial t} + \frac{\partial \langle u_j \rangle k}{\partial x_j} = -\frac{\partial}{\partial x_j}\left(\frac{1}{\rho}\left\langle u_j' p' \right\rangle + \left\langle u_j' k' \right\rangle\right) - \left\langle u_i' u_j' \right\rangle S_{ij} - 2\nu \left\langle s_{ij} s_{ij} \right\rangle, \tag{1}$$

where $\langle u_j \rangle$ represents the components of the phase-ensembled-averaged velocity, u_j' and p' are the fluctuating parts of the velocity components and pressure, respectively, and ν is the kinematic viscosity. Here $k' = (1/2)\ u_i' u_i'$ is the instantaneous turbulent kinetic energy, and S_{ij} and s_{ij}

0148-0227/04/2003JC002233$09.00

represents the mean and fluctuating parts of the strain rate, respectively, and is given by

$$S_{ij} = \frac{1}{2}\left(\frac{\partial\langle u_i\rangle}{\partial x_j} + \frac{\partial\langle u_j\rangle}{\partial x_i}\right)$$

and

$$s_{ij} = \frac{1}{2}\left(\frac{\partial u_i'}{\partial x_j} + \frac{\partial u_j'}{\partial x_i}\right).$$

The turbulence production and dissipation rates are defined to be, respectively,

$$P = -\left\langle u_i' u_j' \right\rangle S_{ij}$$

and

$$\varepsilon = 2\nu\langle s_{ij}s_{ij}\rangle$$

corresponding to the last two terms in equation (1).

[5] Typical turbulence models that have been used include Prandle's mixing length and *k-l* and *k*-ε models [*Jones and Launder*, 1972; *Launder and Spalding*, 1972]. Mixing-length models represent the Reynolds stress and the energy dissipation rate as a function of the mixing or scale length of the turbulent process. In situations of high Reynolds number and where the turbulence transport terms are negligible, the dissipation rate can be modeled as [*Launder and Spalding*, 1972]

$$\varepsilon = C_D \frac{k^{3/2}}{l}, \tag{2}$$

where l is the length scale of the turbulence and C_D is an empirical constant (~0.09).

[6] The dissipation rate, ε, can also be related to the energy spectrum, $E(\kappa)$, of turbulence in the inertial subrange. Turbulence in this range is approximately isotropic and the energy spectrum has the following form:

$$E(\kappa) = \alpha\varepsilon^{2/3}\kappa^{-5/3}, \tag{3}$$

where $\alpha \sim 1.5$ is an empirical constant and κ is the modulus of the wave number vector. $E(\kappa)$ is also related to the one dimensional Fourier transform of the auto correlation of the lateral or streamwise velocity, ϕ, and it can be shown that in the inertial subrange [*Batchelor*, 1953; *Hinze*, 1959; *Pope*, 2000]:

$$\phi = \frac{18}{55}\alpha\varepsilon^{2/3}\kappa^{-5/3}. \tag{4}$$

The breaking of waves in the surf zone results in an eddy structure which is predominantly two-dimensional (2-D) in character in the wave crests. The largest of these 2-D eddies have dimensions which are of the order of the wave height. As shown by *Nadaoka et al.* [1989], these 2-D eddies breakdown into smaller 3-D eddies while at the same time being advected or diffused into other parts of the wave. As discussed by *Lin and Liu* [1998], the 2-D horizontal vertical motions are highly coherent, suggesting that most of their contributions come from the mean flow motion. Equation (2) and the analysis contained in this paper is directed primarily to the energetic 3-D eddies arising from the decay of these 2-D eddies. This turbulence field can be characterized by both a micro and a macro length scale. The former characterizes the size of the turbulent eddies that dissipate the turbulence to heat, while the macro scale characterizes the size of the eddies that contain the dominant part of the turbulent energy. This latter scale can be used to parameterize turbulent exchange processes through an eddy viscosity or turbulent diffusion coefficient and is hence the subject of the present investigation.

[7] One of the earliest measurement of scale length in turbulence generated by a oscillating grid showed an increase of scale length away from the grid, consistent with diffused transport of turbulence [*E and Hopfinger*,1986]. Using the method of particle image velocimetry, *Chang and Liu* [1999] have estimated dissipation rates in waves breaking in water of intermediate depth. There have also been a limited number of measurements of dissipation and length scale relevant to the surf zone. Field measurements of dissipation rates have been conducted by *Flick and George* [1990] and *George et al.* [1994] using hot film measurement techniques, while *Trowbridge and Elgar* [2001] estimated dissipation rates from velocity data captured using acoustic Doppler probes. Laboratory experiments were conducted by *Ting and Kirby* [1996] and *Pedersen et al.* [1998]. *Ting and Kirby* [1996] have estimated dissipation rates in laboratory spilling waves using LDA measurements of turbulence kinetic energies and an assumed length scale of $0.1h$. *Pedersen et al.* [1998] have reported on the estimation of length scales using temporal correlation analysis of LDA velocity measurements. In all of the above cases relevant to the surf zone, measurements were confined to positions below the effective trough level.

[8] All of the above experiments required the separation of turbulence velocity fluctuations from wave motions, which are up to 3 orders of magnitude more energetic. A phase-averaging technique for separating these two contributions to the measured flow field is employed by most investigators in the case of monochromatic waves. However, as the method depends on wave repeatability, *Svendsen* [1987] warns against errors that may be introduced because of small variations in wave period that may occur even in controlled laboratory conditions. The method is still considered superior to alternative techniques, such as the moving-average method, with *Nadaoka et al.* [1989] finding that this method apparently only calculates the averaged stress produced by small eddies in computing turbulence magnitudes up to two orders of magnitude smaller than that by phase averaging.

[9] In this paper, we present time-averaged estimates of the dissipation rates and length scales over the entire water column, including that portion of the water column that exists in the crest region above the trough level, for spilling waves breaking in a laboratory surf zone. Dissipation rates were estimated from the time-averaged wave number spectrum of the lateral turbulence velocities using equation (4). Length scales were estimated using the estimated dissipation rate and turbulent kinetic energy measurements in

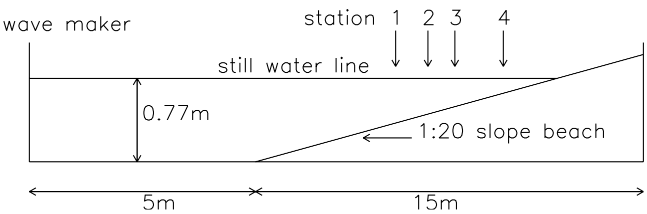

Figure 1. Flume dimensions and measurement positions. Velocity flow fields in spilling waves were measured at stations 1, 2, and 3, which are located at 0.24 m, 1.22 m, and 2.21 m, respectively, from the breakpoint.

equation (2). The time-averaged wave number spectrum was estimated from a series of instantaneous velocity flow field measurements. These velocity flow fields were measured using video imaging and analyzed using digital correlation image velocimetry (DCIV). By tracking the motion of neutrally buoyant particles, as well as bubble structures within the crest of the wave, we were able to measure velocities well into the crest of the wave. The validation of this measurement, including a discussion of the statistical convergence of the ensemble averaging method in addition to other results from the same experiment, is given by *Govender et al.* [2002b]. The experimental setup and procedures are presented in section 2, followed by the results and discussion in section 3.

2. Experimental Conditions and Procedures

[10] Experiments on regular two-dimensional waves were conducted in a 20 m long glassed walled flume, located in the Coastal Engineering Laboratory, CSIR, Stellenbosch, South Africa. Figure 1 shows a schematic of the flume together with dimensions and measurement positions. Waves were generated by means of a hinged paddle driven by an electric motor. The flume was also fitted with a 1:20 slope beach on which wave breaking occurred. Measurements were restricted to positions along the flume beyond the breakpoint. Video measurements of the instantaneous velocity flow fields in spilling waves were conducted at stations 1, 2, and 3. Regular waves having a deep water wave height of 16 cm and a frequency of 0.9 Hz were used in the experiment. Table 1 summarizes the wave characteristics at the measurement stations 1, 2, and 3.

[11] The velocity vector field of the wave was measured using a technique known as Digital-Correlation-Image-Velocimetry (DCIV). The fluid velocity vector field was estimated by tracking the displacement of a small region of the seeded and aerated flow. The experimental setup for this purpose was as follows: A longitudinal section of the flume was illuminated with a strobed light sheet and the aeration and illuminated particles were imaged using a progressive scan CCD camera connected to a PC frame grabber. Two video images of the aerated and seeded flow, which were separated in time by a few milliseconds, were captured. The instantaneous velocity field was then obtained as follows: An interrogation window, of size 24 $\times$ 24 pixels (corresponding to a sampling window of $\sim$1 cm $\times$ 1 cm in the fluid medium), was placed at the bottom left corner of the image. The subimage within the interrogation window was then cross-correlated (implemented in the frequency domain) with the corresponding subimage in the second image. The position of the peak in the cross correlation, provided a measure of the displacement of the structure in the second subimage with respect to that in the first. The velocity at the location of the interrogation window was then obtained by dividing the displacement of the structure in the subimages by the time interval between the images. The interrogation window was then moved horizontally and vertically in steps of 6 pixels and the above procedure was repeated. This results in velocity estimates at intervals of $\sim$0.25 cm. More details of the experimental setup and the imaging and computational procedures are given by *Govender et al.* [2002a].

[12] For the purpose of spectral analysis instantaneous velocity flow fields were measured using a sampling time (interval between two consecutive images) of 1 ms. Since the camera was capable of imaging only a 30 cm section of the wave in order to provide an acceptable spatial resolution, it was necessary to image the wave in sections. The camera was arranged to image a 30 cm section of the flow field at each station. A TTL trigger signal obtained from the wave generator made it possible to capture an image at a particular phase. By adjusting the capture delay, with respect to the trigger pulse, a sequence of 50 image pairs were captured at each of 10 equally spaced phase intervals and resulting in 50 instantaneous velocity fields at each wave phase.

[13] Figure 2 shows a sample of the flow field in the crest of the spilling wave at station 3. It is clear from Figure 2 that there are a number of regions where no results are shown, because of the lack of sufficient seed or aeration structure in the corresponding fluid volume. In order to perform spectral

Table 1. Characteristics of the Spilling Waves[a]

	x-x_b, cm	H, cm	d, cm	h, cm	H/h	h/h_b
Station 1	24	16.5	21.8	21.2	0.78	0.959
Station 2	122	9.4	16.9	16.8	0.56	0.760
Station 3	221	6.5	11.9	12.6	0.51	0.570

[a]Definitions are as follows: H, h, and h_b are the local wave height, mean water depth, and mean water depth at breakpoint, respectively; d is the local still water depth, and x-x_b is the distance beyond the breakpoint.

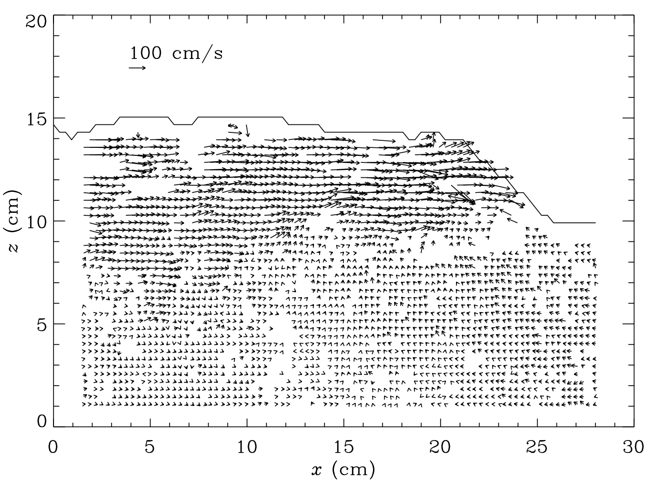

Figure 2. Sample of an instantaneous velocity flow field in the crest of the spilling wave at station 3.

analysis using the standard fast Fourier transform (FFT) routines it is necessary to interpolate the measured flow field in those regions where results are not available. As Figure 2 indicates, interpolation was required over ~10% of the area. The size of the voids in Figure 2 is roughly of the order of 2 cm. Thus the interpolation would result in a lower estimate of the turbulent kinetic energy for wave numbers greater than $\sim\pi$ cm^{-1} (corresponding to wavelengths less than 2 cm) by approximately 10%.

[14] Spectral analysis of the velocity field was performed using a one-dimensional FFT of each row of the horizontal (also referred to as lateral, longitudinal, or streamwise) velocities in each flow field. The spectra of each instantaneous flow field, 50 for a given phase, were then averaged to give a phase-ensemble-averaged spectrum. With the ensemble average this was repeated for the other phases.

[15] The peak nondimensional horizontal turbulence intensities, $u'/(gh)^{1/2}$, occurring in the crest of the wave at stations 1, 2, and 3, were found to be 0.1, 0.54, and 0.53, respectively [*Govender et al.*, 2002b]. It has been shown by *Govender et al.* [2002b] that the computation of the turbulence velocities converges for an ensemble number that is greater than 40. Thus the averaging over 50 instantaneous spectra is guaranteed to ensure convergence of the phase-ensemble-averaged spectra. Finally the phase-ensemble-averaged spectra were averaged to give a time-averaged spectrum.

3. Results and Discussion

[16] Samples of the time averaged wave number spectra of the turbulence velocities at various depths at stations 1 and 2 are shown in Figures 3 and 4, respectively. Also shown in Figures 3 and 4 are the least squares fitted line to the upper end of the spectra. The spectrum (not shown) at station 3 was similar to that shown in Figure 4. Figures 3 and 4 clearly show the $-5/3$ dependence for wave numbers in the range $0.3 < \log(\kappa) < 0.7$. In fact, there are three regimes that are clearly visible in Figures 3 and 4, namely

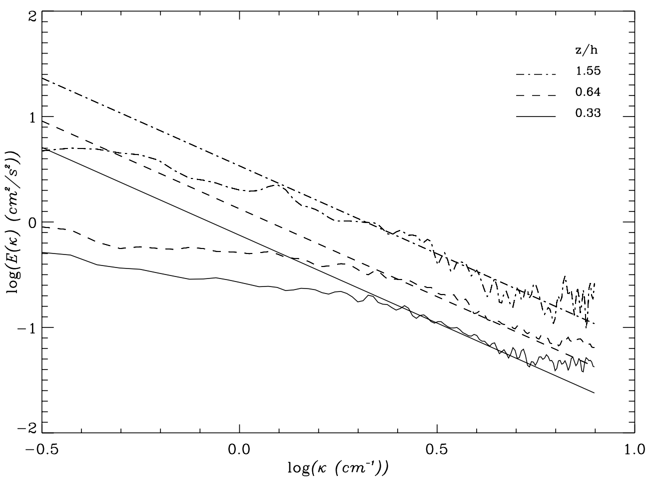

Figure 3. Time-averaged wave number spectra of the turbulence velocities at vertical positions of $0.33h$, $0.64h$, and $1.55h$ above the bed, at station 1. The $-5/3$ slope line fitted to the spectra at each depth (straight lines) is also shown.

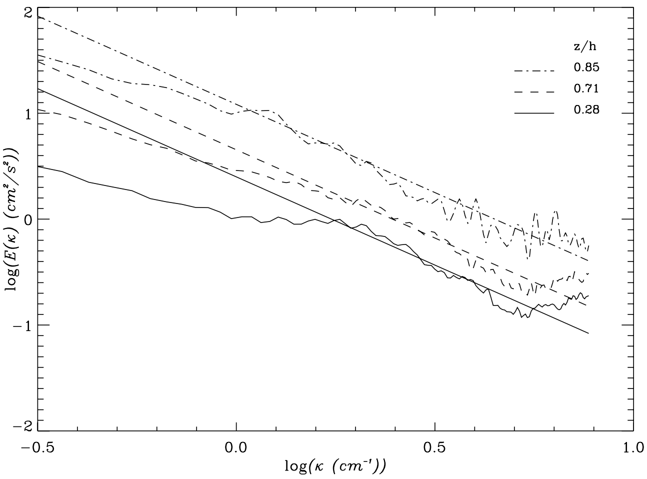

Figure 4. Time-averaged wave number spectra of the turbulence velocities at vertical positions of $0.28h$, $0.71h$, and $0.85h$ above the bed, at station 2. The $-5/3$ slope line fitted to the spectra at each depth (straight lines) is also shown.

(1) $E(\kappa) \propto \kappa^a$, where "a" is some unspecified number, for $\log(\kappa) < 0.3$; (2) $E(\kappa) \propto \kappa^{-5/3}$, for $0.3 < \log(\kappa) < 0.7$, and (3) $E(\kappa)$ is almost constant, very much like white noise, for $\log(\kappa) > 0.7$.

[17] Approximating κ by $2\pi f/u'_{\rm rms}$, region 2 above corresponds to an average frequency range of 1.7Hz $< f <$ 4.3Hz, where a depth averaged value of $u'_{\rm rms}$ of 3.3, 7.0, and 6.0 m/s have been used at station 1, 2, and 3, respectively [*Govender et al.*, 2002b]. Region 3, corresponding to the noise range, translates to a frequency range $f > 6$ Hz. The above subdivisions compares favorably with measurements conducted in the swash zone by *Raubenhiemer et al.* [2004], who estimated the inertial subrange to be 1.5 Hz $< f <$ 4.5Hz and a noise range $f >$ 6 Hz.

[18] There is not a clear distinction between the three regions mentioned above. Energy dissipation rates were then estimated from the y-intercept of the least squares fitted line to the spectra in the range $0 < \log(\kappa) < 0.7$, corresponding approximately to region 2 mentioned above. Figure 5 shows the nondimensionalized energy dissipation rate, $\varepsilon h/(gh)^{3/2}$, at stations 1, 2, and 3. At station 1, dissipation was confined mostly to the upper part of the water column. This is due to the incipient wave breaking at this station. In the rest of the water column dissipation is minimal. Dissipation rates at stations 2 and 3 are distributed through the water column, with peak values occurring in the crest of the waves, and decreasing almost exponentially as the bed is approached. Shown in Figure 6 are the dissipation rate measurements made by *Ting and Kirby* [1996] Test 1, at three stations in laboratory spilling waves breaking on a 1:35 slope beach. Also shown in Figure 6 are the present measurements made at station 3. The present measurements are seen to be of a similar magnitude to those of *Ting and Kirby* [1996] at positions below the trough level. Figure 6, however, clearly illustrates that the dissipation rate below the trough level is only a small proportion of the total TKE dissipated through the water column. The depth integrated dissipation rates at stations 1, 2, and 3 are shown in Table 2.

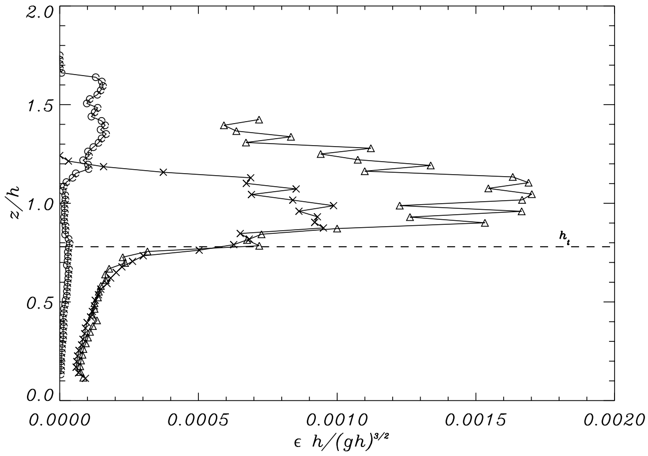

Figure 5. Nondimensional dissipation rates as a function of distance above the bed at stations 1 (circles), 2 (triangles), and 3 (crosses). The position of the mean trough level (z/h) at stations 1, 2, and 3 are 0.77, 0.8, and 0.78, respectively, and a single dashed line representing the mean trough position for all three stations is shown.

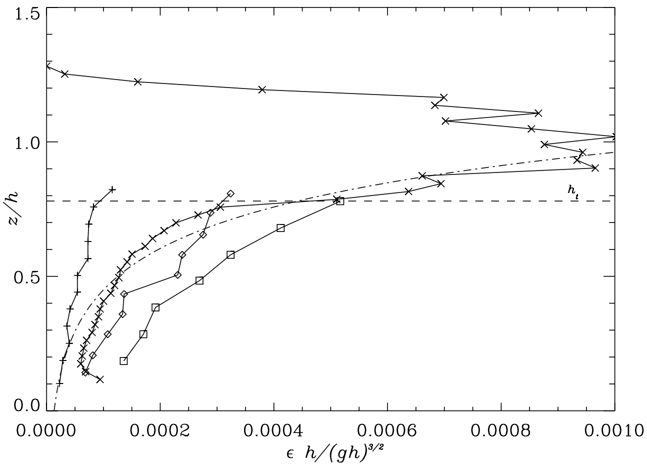

Figure 6. Dissipation rates as a function distance above the bed at station 3 (crosses) compared with dissipation rates by *Ting and Kirby* [1996] at positions where h/h_b is 0.879 (pluses), 0.744 (diamonds), and 0.563 (squares). The dash-dotted line represents the exponentially fitted curve to the present measurements at station 3, and the dashed line represents the mean trough level at station 3. (Modified from *Ting and Kirby* [1996], with permission from Elsevier.)

Table 2 shows that the total depth integrated dissipation rates ranges from ~300 to ~1700 cm^2/s^3. These results are consistent with field measurements conducted by *Flick and George* [1990] and *Raubenhiemer et al.* [2004]. As may be seen from Table 1, an estimated 14% to 20% of the TKE is dissipated below the trough level in the present measurement set. These values are somewhat higher than the earlier estimates made by *Svendsen* [1987], who found that only between 2% to 6% of the energy loss in the breaker is dissipated below the trough level, but still support the earlier observation.

[19] An exponential curve of the form

$$\varepsilon(z) = \varepsilon_s \exp[\beta(z/h - 1)] \tag{5}$$

with $\beta = 4.5$ representing the decay constant, has been fitted to the dissipation rate measured at station 3 and is also shown in Figure 6. As discussed by *Mocke* [2001], a local equilibrium between dissipation and diffusion of TKE is associated with an exponential decay in the rate of dissipation in the form

$$\varepsilon = \varepsilon_s \exp\left[\frac{3}{2}(z-h)l\right]. \tag{6}$$

Assuming a representative value of the length scale of l = 0.3h (although we show below that the length scale is variable across the depth), the expression in equation (6) above is associated with a decay constant of the order 5. This is relatively close to the value of 4.5 found for the fit shown in Figure 6 and appears to further reinforce the interpretation that there is turbulent diffusion downward from the near surface wave roller.

[20] A modeling exercise [*Mocke*, 2001] based on the same experimental configuration indicates that the intensity of the boundary layer turbulence is very much smaller than that due to wave breaking. Thus the surf zone turbulence arises primarily from the transfer of energy due to wave breaking and it is reasonable to consider that the rate of production of turbulent kinetic energy should be of a similar magnitude. Shown in the same Table 2 are the values of wave energy dissipation (D_w) rates estimated from wave height measurements across the surf zone [*Govender et al.*, 2002b], and predictions based on the bore approximations (D'_w) of waves in the surf zone. The cross-shore distribution of wave energy dissipation rates was estimated using the fact that the negative of the spatial gradient in energy flux of the waves is equal to the wave energy dissipation rate, i.e.,

$$-\frac{dcE_w}{dx} = D_w, \tag{7}$$

where $c = (gh)^{1/2}$ and $E_w = \rho g H^2/8$ have been used. The wave energy dissipation rate is then proportional to the cross-shore distribution of the gradient in wave height. The estimate of the cross-shore distribution of the gradient in wave height for this particular experiment is shown in Figure 7. The left-hand side of equation (7) has been evaluated using the measured wave height data and smoothed by means of a moving average filter. It is clear from Table 2 that the measured depth integrated turbulence dissipation rate is much smaller than the estimated wave energy dissipation rate, which is in turn expected to give a

Table 2. Comparisons of Turbulence and Wave Energy Rates Per Unit Horizontal Area[a]

Position	ε'_l	ε'_u	ε'_{tot}	D_w	D'_w
station 1	36.53	215.81	252.34	14147.23	46770.01
station 2	312.87	1410.42	1723.29	15742.29	10912.53
station 3	114.47	476.53	591.00	6816.62	4810.84

[a]Units are in cm^3/s^3. Definitions are as follows: ε'_l, ε'_u, and ε'_{tot} are the depth integrated dissipation rates below mean trough level, above mean trough level and the total depth integrated dissipation rate, respectively. D_w and D'_w are the total wave energy dissipation rates estimated from wave height analysis and bore model prediction, respectively.

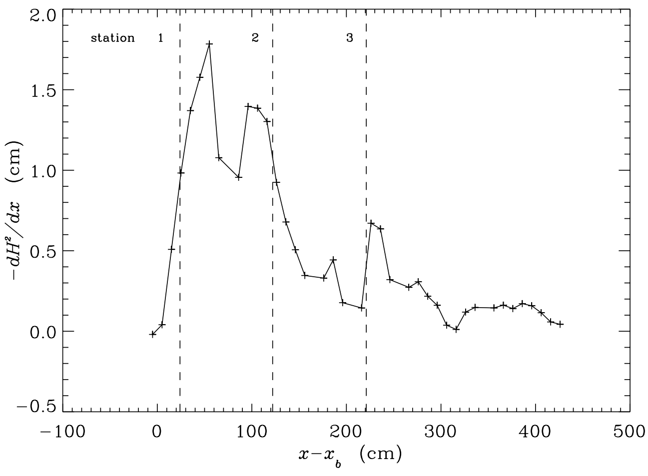

Figure 7. Cross-shore distribution of the gradient in measured wave heights. The position of stations 1, 2, and 3 are represented by the dashed lines.

good approximation of the local turbulence production rate. This implies that the major part of the turbulence is not dissipated at the position of turbulence and is possibly transported and dissipated elsewhere in the surf zone.

[21] Estimates of wave energy dissipation rates based on the bore approximation [*Battjes and Janssen*, 1978], i.e.,

$$D'_w \propto \frac{1}{4} f \rho g \frac{H^3}{h}, \tag{8}$$

where f is the frequency of the wave and the other symbols have their usual meaning, indicate values at stations 2 and 3 that are also very much greater than the spectrally estimated turbulence dissipation rate.

[22] A contributory factor for this discrepancy arises from the inability of either the energy flux or bore approximations to quantify the roller dynamics, particularly through the wave transition zone. This is illustrated by *Mocke et al.* [2000], where a roller model applied to the plunging wave case in the same experiment shows appreciable differences between predicted roller and wave energy dissipations across the surf zone. The approximately order of magnitude differences observed in Table 2 are, however, much higher and imply a lack of local balance between the depth integrated TKE production and dissipation rates. As observed by *Ting* [2001] and *Chang and Liu* [1999] in measurements mainly confined to the area below the trough level, TKE is transported shoreward because of turbulent velocity fluctuations and wave velocities. This transport mechanism is expected to be even more apparent in the region above the wave trough level where *Govender et al.* [2002b] have measured mass flux and velocity fields having strong onshore components. These results suggest the transport of an excess supply of TKE production shoreward of the measurement section, in the region of the swash zone. Although analysis and measurement limitations may have contributed to the computed dissipation surplus, it is likely that inshore transport by the wave roller is an important mechanism. This has particular significance for surf zone model studies where the wave energy loss is frequently an important source term for turbulence production in the turbulent kinetic energy transport equation. A proper analysis should in principle involve the transport equation for the dissipation rate, however the analysis presented here is simple and practical, and gives a first hand insight into the behavior of the dissipation rate.

[23] The length scale, l, was estimated using equation (2) and the measured dissipation rates and turbulent kinetic energies. A comment on the applicability of equation (2) is warranted. It has been suggested by *Launder and Spalding* [1972] that the value of C_D may need to deviate from the accept value of 0.09 where there is a local imbalance of TKE production and dissipation. However in the absence of any definitive advice, and for the sake of consistency, the accepted value is retained. Recognizing that any inconsistencies arising out of the use of equation (2) will result in the estimated length scale deviating from its true value, comparisons with estimates from other published studies are discussed below. It is further noted that in the present analysis the estimated dissipation rates are not influenced by the use of equation (2).

[24] *Govender et al.* [2002b] have previously described the turbulent kinetic energy measurements, but for completeness, the results are also shown in Figure 8. Also shown in Figure 8 are measurements of turbulent kinetic energy by *Ting and Kirby* [1994] and *Cox et al.* [1994], which are very similar to measurements at stations 2 and 3 presented here. Figures 9, 10, and 11 show the resulting length scales at stations 1, 2, and 3, respectively. Stations 1 and 3 show a general increase of length scale, from the wave crest downward.

[25] The increase in length scale from the crest downward is consistent with earlier findings of *E and Hopfinger* [1986], who found that turbulence diffused away from an oscillating grid, thus supporting the notion of the surface wave roller as the turbulence source. Near the bed, the length scale ranges from $0.1h$ to $0.4h$. Station 3 also shows a decrease in length scale toward the bed. This is due to the increased dissipation rate in the bottom boundary layer and

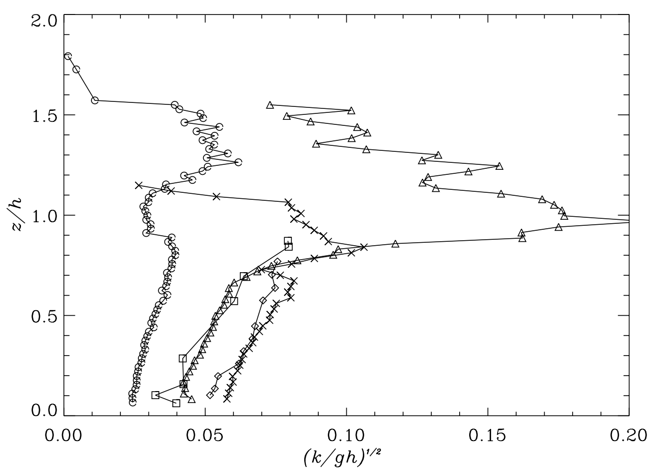

Figure 8. Turbulent kinetic energies as a function of distance above the bed at stations 1 (circles), 2 (triangles), and 3 (crosses). Also shown are measurements by *Ting and Kirby* [1994] (open diamonds) and *Cox et al.* [1994] (open squares) for positions where H/h ~0.7. (Modified from *Ting and Kirby* [1994], with permission from Elsevier.)

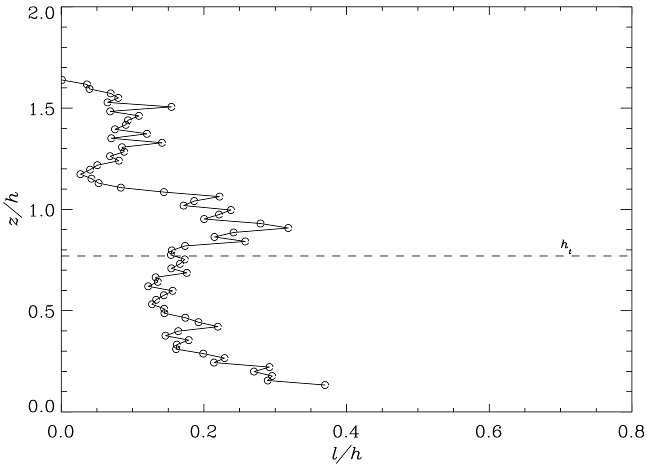

Figure 9. Length scale as a function of distance above the bed at station 1. The dashed line represents the position of the mean trough level.

the confining influence of the bed on the eddy structures. The measurement of length scales at positions below the trough level are consistent with those of *Pedersen et al.* [1998] and others (see *Ting and Kirby* [1996] for a summary of other measurements).

[26] The behavior of the length scale at station 2 is different, being almost constant below the trough level and increasing to $\sim 0.4h$ above. This is probably due to the fact that at station 2 the wave is in the transition zone before the roller is fully developed. A comparison of the wave characteristics at stations 2 and 3, indicates a significantly higher value of H/h at station 2. This, coupled with the premise that l/h scales as H/h, implies a higher value of l/h at station 2. This is certainly the case for positions above the approximate trough level. Through an examination of the cross-shore distribution of depth averaged turbulent kinetic energy in a number of plane slope experiments, *Mocke* [2001] speculates that the transition region for roller development extends to approximately 75% of the break point water depth. Both, stations 1 and 2, fall in this region.

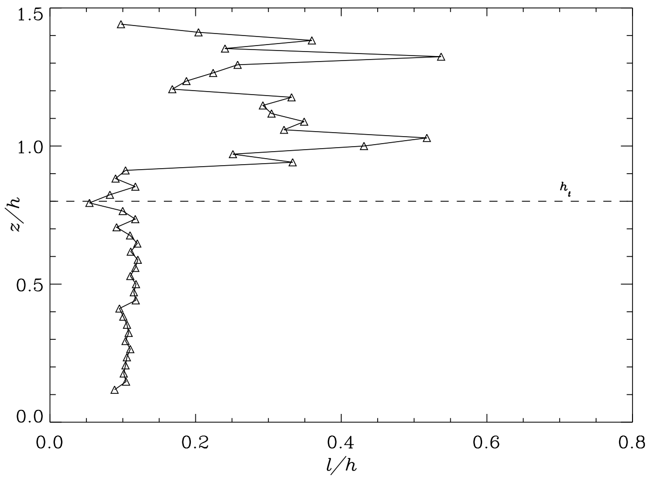

Figure 10. Length scale as a function of distance above the bed at station 2. The dashed line represents the position of the mean trough level.

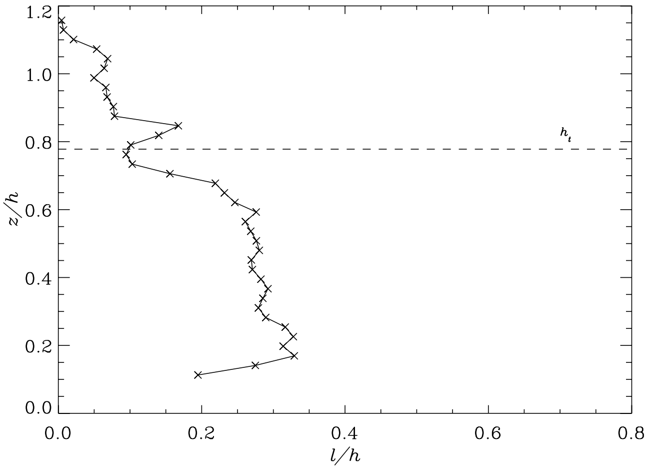

Figure 11. Length scale as a function of distance above the bed at station 3. The dashed line represents the position of the mean trough level.

This is further explored by *Govender et al.* [2002b] with reference to actual roller area measurements, illustrating a progressive increase in size up to the region of station 3. The principal intercomparison should be between stations 2 and 3, as turbulence intensities and dissipation at station 1 are much less significant. At station 2 both the turbulent kinetic energy and dissipation rates are much higher than for station 3 above the trough level. Although dissipation rates are similar at both stations below the trough level, TKE at station 3 is higher. This would suggest higher penetration downward of surface generated TKE at the most shoreward station, and hence the larger and progressively increasing length scales.

4. Conclusion

[27] The instantaneous velocity flow fields, measured using digital correlation image velocimetry (DCIV), have been analyzed to estimate the turbulence dissipation rates and length scales in spilling waves breaking on a 1:20 slope beach. Measurements were presented through the water column for three positions in the laboratory surf zone.

[28] The dissipation rates were estimated from the wave number spectrum in the inertial subrange range. Dissipation rates were found to peak in the crests of the waves and decrease almost exponentially toward the bed. Depth integrated dissipation rates below the trough level were found to compare well with previous measurements and to be only around 14% to 20% of the total dissipation through the water column. The finding that the total depth integrated turbulent kinetic energy dissipation rates are significantly smaller than the measured wave energy flux derived dissipation rates suggests that a considerable proportion of TKE production is transported landward by the wave roller.

[29] Length scales of 3-D isotropic turbulence showed an increasing trend away from the wave crest area and were of similar magnitude to previous published estimates. A peak length scale of $\sim 0.4h$ was found to occur just above the bottom boundary layer, consistent with a number of previous investigations. The results confirm the near surface wave roller as the primary turbulence source under breaking

waves. A significant contribution made in the current investigation is the measurement of the energy dissipation rate and length scale over extended regions that span the entire water column and hence should be useful for future surf zone turbulence modeling initiatives.

[30] **Acknowledgment.** The significant contribution by the anonymous reviewers, as well as the provision of the CSIR experimental facilities, is gratefully acknowledged.

References

Batchelor, G. K. (1953), *The Theory of Homogenous Turbulence*, Cambridge Univ. Press, New York.

Battjes, J. A., and J. P. F. M. Janssen (1978), Energy loss and setup due to breaking of random waves, paper presented at 16th International Conference on Coastal Engineering, Am. Soc. of Civ. Eng., Hamburg, Germany.

Chang, K.-A., and P. L.-F. Liu (1999), Experimental investigation of turbulence generated by breaking waves in water of intermediated depth, *Phys. Fluids*, *11*, 3390–3400.

Cox, D. T., N. Kobayashi, and A. Okayasu (1994), Vertical variations of fluid velocities and shear stress in surf zones, paper presented at 24th International Conference on Coastal Engineering, Am. Soc. of Civ. Eng., Kobe, Japan.

E, X., and E. J. Hopfinger (1986), On the mixing across an interface in stably stratified fluid, *J. Fluid Mech.*, *166*, 227–244.

Flick, R. E., and R. A. George (1990), Turbulence scales in the surf and swash, paper presented at 22nd International Conference on Coastal Engineering, Am. Soc. Civ. Eng., Delft, Netherlands.

George, R., R. E. Flick, and R. T. Guza (1994), Observations of turbulence in the surf zone, *J. Geophys. Res.*, *99*(C1), 801–810.

Govender, K., M. J. Alport, G. Mocke, and H. Michallet (2002a), Video measurements of fluid velocities and water levels in breaking waves, *Phys. Scr. T*, *97*, 152–159.

Govender, K., G. P. Mocke, and M. J. Alport (2002b), Video-imaged surf zone wave and roller structures and flow fields, *J. Geophys Res.*, *107*(C7), 3072, doi:10.1029/2000JC000755.

Hinze, J. O. (1959), *Turbulence*, McGraw-Hill, New York.

Jones, W. P., and B. E. Launder (1972), The prediction of laminarization with a two equation model of turbulence, *Int. J. Heat Mass Transfer*, *15*, 301–314.

Launder, B. E., and D. B. Spalding (1972), *Mathematical Models of Turbulence*, Academic, San Diego, Calif.

Lin, P., and P. L.-F. Liu (1998), Turbulence transport, vorticity dynamic, and solute mixing under plunging breaking waves in surf zone, *J. Geophys. Res.*, *103*(C8), 15,677–15,694.

Mocke, G. P. (2001), Structure and modeling of surf zone turbulence due to wave breaking, *J. Geophys. Res.*, *106*(C8), 17,039–17,057.

Mocke, G. P., K. Govender, M. J. Alport, F. Smit, and G. Diederich (2000), Modelling of digitally imaged water levels and flowfields, 27th International Conference on Coastal Engineering, Am. Soc. of Civ. Eng., Sydney, Australia.

Nadaoka, K., M. Hino, and Y. Koyano (1989), Structure of the turbulent flow field under breaking waves in the surf zone, *J. Fluid Mech.*, *204*, 359.

Pedersen, C., R. Deigaard, and J. Sutherland (1998), Measurements of the vertical correlation in turbulence under broken waves, *Coastal Eng.*, *35*, 231–249.

Pope, S. B. (2000), *Turbulent Flows*, Cambridge Univ. Press, New York.

Raubenhiemer, R., S. Elgar, and R. T. Guza (2004), Observations of swash zone velocities: A note on friction coefficients, *J. Geophys. Res.*, *109*, C01027, doi:10.1029/2003JC001877.

Svendsen, I. A. (1987), Analysis of surf zone turbulence, *J. Geophys. Res.*, *92*(C5), 5115–5124.

Ting, F. C. K. (2001), Laboratory study of wave turbulence velocities in a broad-banded wave surf zone, *Coastal Eng.*, *43*, 183–208.

Ting, F. C. K., and J. T. Kirby (1994), Observation of undertow and turbulence in a laboratory surf zone, *Coastal Eng.*, *24*, 51–80.

Ting, F. C. K., and J. T. Kirby (1996), Dynamics of surf-zone turbulence in a spilling breaker, *Coastal Eng.*, *27*, 131–160.

Trowbridge, J., and S. Elgar (2001), Turbulence measurements in the surf zone, *J. Phys. Oceanogr.*, *31*, 2403–2417.

M. J. Alport, School of Pure and Applied Physics, University of KwaZulu-Natal, King George V Avenue, Durban, 4001, South Africa. (alport@ukzn.ac.za)

K. Govender, Department of Physics, University of KwaZulu-Natal, Private Bag X54001, Durban, 4000, South Africa. (govenderks@ukzn.ac.za)

G. P. Mocke, Marine Works Unit, Dubai Municipality, P.O. Box 67, Dubai, United Arab Emirates. (marineu@dm.gov.ae)